Flow Dichroism as a Reliable Method to Measure the Hydrodynamic Aspect Ratio of Gold Nanoparticles

Naveen Krishna Reddy,[†] Jorge Pérez-Juste,[‡] Isabel Pastoriza-Santos,[‡] Peter R. Lang,[§] Jan K. G. Dhont,[§] Luis M. Liz-Marzán,[‡] and Jan Vermant[†,*]

[†]Department of Chemical Engineering, K.U. Leuven, W. de Croylaan 46, B-3001 Leuven, Belgium, [‡]Departamento de Quimica Fisica and Unidad Asociada CSIC, Universidade de Vigo, 36310,Vigo, Spain, and [§]Institute for Festkorperforschung Forschungszentrum, Juelich, D-52425 Juelich, Germany

ABSTRACT Particle shape plays an important role in controlling the optical, magnetic, and mechanical properties of nanoparticle suspensions as well as nanocomposites. However, characterizing the size, shape, and the associated polydispersity of nanoparticles is not straightforward. Electron microscopy provides an accurate measurement of the geometric properties, but sample preparation can be laborious, and to obtain statistically relevant data many particles need to be analyzed separately. Moreover, when the particles are suspended in a fluid, it is important to measure their hydrodynamic properties, as they determine aspects such as diffusion and the rheological behavior of suspensions. Methods that evaluate the dynamics of nanoparticles such as light scattering and rheo-optical methods accurately provide these hydrodynamic properties, but do necessitate a sufficient optical response. In the present work, three different methods for characterizing nonspherical gold nanoparticles are critically compared, especially taking into account the complex optical response of these particles. The different methods are evaluated in terms of their versatility to asses size, shape, and polydispersity. Among these, the rheo-optical technique is shown to be the most reliable method to obtain hydrodynamic aspect ratio and polydispersity for nonspherical gold nanoparticles for two reasons. First, the use of the evolution of the orientation angle makes effects of polydispersity less important. Second, the use of an external flow field gives a mathematically more robust relation between particle motion and aspect ratio, especially for particles with relatively small aspect ratios.

KEYWORDS: gold rod · gold decahedron · transmission electron microscopy · depolarized dynamic light scattering · Brownian motion · flow dichroism · Jeffery orbits

Nonspherical nanoparticles are being extensively used as basic building blocks to construct large-scale structures having controlled shapes and sizes, with tailored chemical and mechanical properties, all the way to design devices with unique optical and electrical properties.[1] Promising novel applications of nano-sized nonspherical particles include those that use localized surface plasmon resonances (LSPRs),[2] exploit single-electron tunneling,[2] or focus on high strength and conductivity in nanocomposite polymers.[3] Other applications use the nanoparticles as fluorescence enhancers,[4] as a source for strong local heating,[5] as waveguides for subwavelength photonics integration,[6] or for their use in high-density recording media.[7] Another important reason for studying nonspherical particles is that the colloidal domain is dominated by nonspherical particles, where 90% of particles found in nature are disks, 9% are rods, and the remaining 1% includes all the other shapes. However, most research so far has focused on spherical colloids and microparticles. Even biological particulate systems are dominated by anisotropic shapes, such as red blood cells, which are oblate, or rod-like actin and microtubules, which are used for strengthening the cells' cytoskeleton.[8,9] In the majority of applications, either during the production process or in the final product, nanoparticles are suspended in a fluid. A knowledge of hydrodynamic dimension and the associated polydispersity is essential in understanding the effect of nonspherical nanoparticles on phenomena such as self-assembly[10] and directed self-assembly,[11] as well as the dynamics of phase transitions.[12]

Electron microscopy (EM) is used extensively to determine dimensions of nonspherical nanoparticles. The characterization of nanoparticles by electron microscopy is based on generating an image of the particles by collecting secondary or backscattered electrons in the case of scanning electron microscopy (SEM) and from transmitted electrons in the case of transmission electron microscopy (TEM).[13] For TEM a drop of suspension containing nanoparticles is dried on a grid prior to imaging. Due to small sample volume, tens of EM images have to be processed to get reasonable statistics on the nanoparticle dimensions. This process is time-consuming and expensive; therefore most often only a limited number of particles is counted, and the statistics are typically poor. The size obtained from electron microscopy gives a

* Address correspondence to jan.vermant@cit.kuleuven.be.

Received for review March 18, 2011 and accepted May 5, 2011.

Published online May 05, 2011
10.1021/nn201033x

physical dimension of the particle in the dried state and does not necessarily represent the nanoparticles in suspension, where for example the electroviscous effects, adsorbed polymer, surfactant, or hydration layers change the effective hydrodynamic dimensions.[14]

The present work compares methods to analyze the hydrodynamic properties of nonspherical gold nanoparticles. More specifically, we focus on depolarized dynamic light scattering (DDLS) and flow-induced dichroism. Although the elastic scattering for nanosized particles is weak, nonspherical gold nanoparticles exhibit an anisotropy in polarizability due to excitation of directional LSPRs. In nanorods, two distinct LSPRs can be excited, related to transverse and longitudinal electron oscillations, which lead to both scattering and absorption of light.[5,15] The presence of LSPR causes the polarization of the scattered light to depend on the orientation of the particles.[15] This dependence on orientation can be exploited in DDLS to obtain the translational (D_t) and rotational (D_r) diffusion coefficients, by measuring time−autocorrelation functions of the scattered light with polarization parallel and perpendicular to the incident beam polarization. These two diffusion coefficients are related to hydrodynamic dimensions (length and width), although for short particles the effect of finite length is not trivial to account for. The LSPRs also lead to an optical anisotropy for an aligned suspension of nanoparticles and induce an intrinsic contribution to anisotropy of the refractive index tensor, which can be measured even when the elastic scattering, due to the small particle size, is weak.

DDLS investigates the fluctuations in orientation and position due to Brownian motion in a randomly oriented suspension, whereas the optical responses from an oriented suspension would be different. On the contrary, in rheo-optical measurements, the transient optical response of a suspension subjected to flow is used to measure the particle properties.[16] For example, it has been shown that the time evolution of the polarized UV−vis absorption can be used to obtain a hydrodynamic dimension.[17] Here we use an even simpler polarimetric method to measure the time evolution of the anisotropy in the refractive index tensor. A well-defined flow field is applied to control the motion of the particles.[16] Nonspherical particles in flow tumble due to a difference in torque between the two ends of the particle, provided that the local velocity gradients are high enough, such that the motion is determined solely by the hydrodynamic forces. Provided that the convective force overwhelms the force associated with the Brownian motion (as characterized by the Péclet number), when the flow is started up, the time-dependent optical response of the particles will show a damped oscillatory behavior due to the effect of the tumbling motion of the particles on the overall orientation distribution function (ODF). The tumbling period of the ODF depends on the hydrodynamic aspect ratio of the particles. Differences in tumbling periods of the individual particles due to different particle aspect ratios lead to phase mixing, which dampens the optical response of the integrated ODF in time to a steady-state value. The associated polydispersity in aspect ratio of nanoparticles can be extracted by analyzing the decay of optical response of the ODF due to phase mixing. The challenges for using this method for nanoparticles are (a) sufficient anisotropic scattering intensity or absorption and (b) sufficiently high Péclet number.

In the present work we have focused on two different shapes, gold nanorods (Au-nanorod) and decahedral gold nanoparticles (Au-deca). The gold nanorod samples were suspended in aqueous solution and stabilized by the surfactant cetyl trimethylammonium bromide (CTAB). The different decahedral gold nanoparticle samples obviously had the same shape, but their average particle sizes are different. These Au-deca particles were stabilized by a layer of polyvinylpyrrolidone (PVP). The details of gold nanoparticle synthesis have been extensively discussed in the literature, so we do not elaborate on them in this article. For DDLS experiments, the gold nanoparticles were dispersed in water so that the Brownian motion of the nanoparticles can be easily detected. On the other hand, for rheo-optical measurements the gold nanoparticles were dispersed in 99.5% glycerol to increase the medium viscosity and to bring the high Péclet number regime into the experimental range. The particles were characterized by electron microscopy, by DDLS studying Brownian dynamics, and finally by a rheo-optical method investigating flow field enforced dynamics. We compare the different methods with respect to the complexity and possible errors during sample preparation, the measurement errors, and the applicability of different methods to rod-like and disk-shaped decahedral gold nanoparticles. By comparing the three methods, we show that the flow dichroism is the most reliable method to determine hydrodynamic aspect ratio of gold nanoparticles with aspect ratios in the range between 0.1 and 10.

RESULTS

Electron Microscopy. For all nonspherical nanoparticles electron microscopy is a suitable method to determine physical dimensions and the associated polydispersity using quantitative image analysis. For TEM, a drop of nanoparticle suspension is placed on a TEM grid and then allowed to dry before placing the grid inside the TEM and establishing vacuum conditions. Images of the nanoparticles are taken by adjusting the electron beam energy, to get optimum contrast. Typical micrographs obtained from electron microscopy of rod-like (Au-nanorod-2) and decahedral (Au-deca-3) nanoparticles

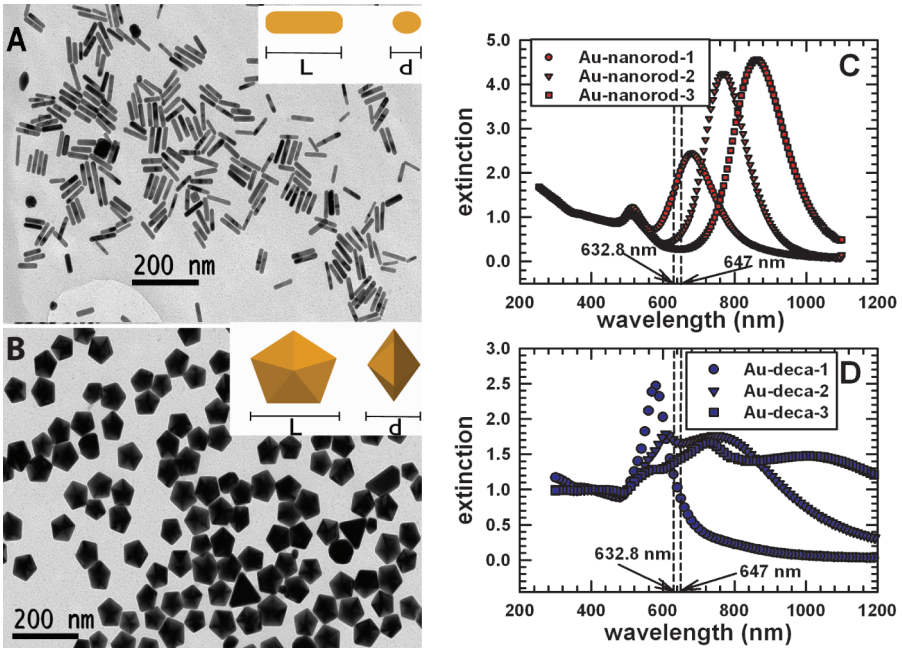

Figure 1. Transmission electron micrographs of nonspherical gold nanoparticles: (A) Au-nanorod-2 and (B) Au-deca-2 (JEOL 1010, 100 kV, scale bars = 200 nm). (C) Extinction spectra for Au-nanorods. (D) Extinction spectra for Au-nanodecas. Insets in (A) and (B) are illustrations defining the measured dimensions, listed in Table 1. All spectra are normalized at 400 nm to facilitate comparison.

are shown in Figure 1A and B. The corresponding geometric nanoparticle dimensions obtained from image analysis using the UTHSCSA ImageTool software[18] are listed in Table 1. For Au-decas only the length of one edge can be measured from the TEM images, but since the Au-decas are decahedral in shape, their aspect ratio should satisfy the golden ratio rule ($d/L = 0.62$; see Figure 1 for the definition of L and d). In Table 1, the length (L) of the Au-deca is calculated as $L = (2L_{side}/10)(50 + 10\sqrt{5})^{1/2}$, where L_{side} is the edge length of a pentagonal bipyramid.[19] The diameter (d) of Au-deca is related to its length by $d = 2(1 - (L/2)^2)^{1/2}$.[19]

The standard error on the arithmetic mean of the geometric aspect ratio (AR) of gold particles with a standard deviation (ρ) is given as $\rho/\sqrt{n}$, where n is the number of particles analyzed to obtain the mean and the ρ. To have a standard error of 1%, 10^4 particles have to be analyzed. In this work we measured 150−200 particles (approximately the number of particles in one image), and to get to 1% standard error, we would need to analyze 50−60 images, which is highly time-consuming. Moreover, the main drawback with this method is that it does not provide direct information about hydrodynamic aspect ratio. It has been proposed that the hydrodynamic aspect ratios can be calculated by adding the estimated thickness of the stabilizing layer to the geometric dimensions obtained from TEM. This empirical method provides an estimate for the hydrodynamic aspect ratio, referred to as P_{TEM}. The stabilizing layer for Au-nanorods is a bilayer of cetyl-trimethylammonium bromide of length 3.2 nm (as determined on a mica surface in the dry state), and it is assumed to be present on all sides of the nanorod.[20,21] For Au-decas the stabilizing layer is made of polyvinylpyrrolidone with a molecular weight of 40 000 Da, which has an estimated thickness of 2 nm.[22]

TABLE 1. Average Geometric Nanoparticle Dimensions (L, d), Geometric Aspect Ratio (AR) Measured from TEM, and Estimated Hydrodynamic Aspect Ratio (P_{TEM})

sample	L (nm)	d (nm)	AR	P_{TEM}
Au-nanorod-1	56.0 ± 6.0	20.0 ± 3.0	2.80 ± 0.84	2.3
Au-nanorod-2	61.0 ± 7.0	18.0 ± 0.5	3.40 ± 0.50	2.7
Au-nanorod-3	66.0 ± 6.0	15.0 ± 2.0	4.40 ± 1.1	3.4
Au-deca-1	73.2 ± 3.3	45.2 ± 2.1	0.62 ± 0.06	0.63
Au-deca-2	170.0 ± 10.0	105.2 ± 6.4	0.62 ± 0.07	0.63
Au-deca-3	292.6 ± 8.5	180.8 ± 5.2	0.62 ± 0.02	0.62

The particle sizes and shapes are such that the particles possess an anisotropic optical response, not only because of the mere geometric dimensions but mainly because of the presence of the LSPR.[23,24] The extinction curves as a function of wavelength are shown in Figure 1C for the different Au-nanorods. As the aspect ratio of the rods is decreased, the plasmon resonance peak shifts to smaller wavelengths and the peak decreases in intensity. However, at the wavelengths used in the light-scattering and rheo-optical experiments, the particles with the smallest aspect ratio show the strongest extinction. As the width of the rods is smaller than 30 nm, most of the extinction will originate from absorption.[24] For the decahedral gold disks, the peaks in the extinction curves in Figure 1D are not as well-defined as in the case of

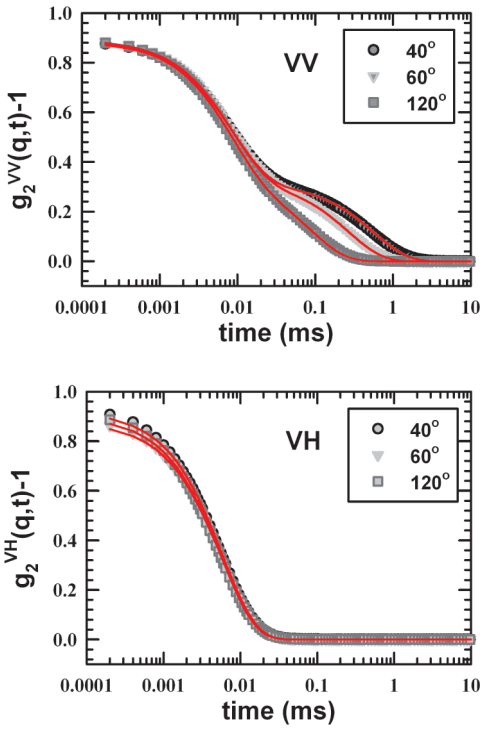

Figure 2. Typical autocorrelation functions for Au-nanorod-1 suspensions recorded in VV and VH modes at 40°, 60°, and 120°. The lines are fits to eq 1 and eq 2.

rods but show sufficient extinction to provide contrast at the wavelengths used in the optical setups.

Depolarized Dynamic Light Scattering. Dynamic light scattering is a standard technique in particle sizing and is typically based on the elastic scattering of light by particles undergoing Brownian motion in a suspension. The time correlation of the intensity fluctuations is a direct measure of the Brownian motion of the particles.[25] For an ensemble of monodisperse particles, the field correlation function is an exponentially decaying function, $g_1(q,t) = \exp\{-\Gamma t\}$, where Γ is the relaxation rate, q is the scattering vector, and t is the correlation time. Γ is related to the particles' translational diffusion. The translational diffusion coefficient (D_t) is related to the particles' effective hydrodynamic radius by the Stokes–Einstein–Sutherland equation.[26,27]

If the particles exhibit sufficiently large shape and/or optical anisotropy, orientational terms will contribute to the relaxation rate.[28−32] This in principle allows the determination of the rotational diffusion coefficient, D_r, provided the state of polarization of the scattered light is considered in the data analysis. Here, we used the depolarized dynamic light-scattering technique to determine both translational and rotational diffusion coefficients for gold nanorods. The analysis of DDLS data used to obtain D_t and D_r for gold nanorods, in the presence of both scattering and absorption, has been previously described in detail by Rodríguez-Fernández *et al.*[33] Briefly, the intensity autocorrelation functions obtained from

TABLE 2. Mean Translational Diffusion (D_t), Mean Rotational Diffusion (D_r) from DDLS, and the Corresponding Hydrodynamic Aspect Ratio Calculated from eq 3,[a]

sample	D_t (1E4) (nm²/ms)	D_r (1/ms)	P_{DDLS}	P_{TEM}
Au-nanorod-1	1.09 ± 0.06	15.1 ± 0.1	1.85 ± 0.65	2.3
Au-nanorod-2	0.99 ± 0.04	15.3 ± 0.2	1.35 ± 0.47	2.8
Au-nanorod-3	0.96 ± 0.02	12.2 ± 0.3	1.55 ± 0.54	3.4

[a] For comparison hydrodynamic aspect ratio calculated by adding stabilizing layer thickness to the TEM data is also shown (P_{TEM}).

light scattered in the so-called vertical−vertical (VV) and vertical−horizontal (VH) modes are not analyzed by CONTIN but better fitted by using eq 1 and eq 2 as explained in ref 33.

$$g_2^{VV}(q,t) - 1 = \beta[A^2 \exp\{-\Gamma_2 t\} + 2AB \exp\{-(\Gamma_2 + \Delta/2)t\} + B^2 \exp\{-(\Gamma_2 + \Delta)t\}] \quad (1)$$

$$g_2^{VH}(q,t) - 1 = \beta' \exp\{-(\Gamma_2 + \Delta)t\} \quad (2)$$

where $\Gamma_2 = 2\Gamma = 2D_t q^2$ and $\Delta = 12D_r$, while $A + B = 1$ are related to the anisotropy of the particles' polarizability. The parameters β and β' account for the nonideality in the light-scattering setup and are smaller than unity.[33] A nonlinear least-squares fitting global algorithm based on an evolution algorithm was used to determine the best fit parameters for eq 1 and eq 2 from 19 correlation functions, corresponding to the VV and VH modes, respectively, at scattering angles spanning from 40° to 130°. In this procedure A, D_t, and D_r are treated as global parameters, while β and β' are allowed to vary between different correlation functions. Examples of the experimentally measured correlation functions are shown in Figure 2 for Au-nanorod-1 in VV and VH modes. For clarity, only the autocorrelation functions for angles of 40°, 60°, and 120° are plotted. Lines in Figure 2 are nonlinear least-squares fits to eq 1 and eq 2.

To derive the hydrodynamic aspect ratio from the experimental data, a relationship between the diffusion coefficients and the hydrodynamic dimension is required. For infinitely thin rods of length L and aspect ratio P_{DDLS} in a fluid of viscosity η and temperature T, slender body results of Boersma and Brenner are available.[34,35] For small aspect ratios, correction factors C_t and C_r are required to account for the relative importance of end effects due to the finite rod length.[36] The modified Brenner equations can be combined to yield an implicit relation between the aspect ratio and the diffusivities:

$$f(P_{DDLS}) = \left\{\frac{9\pi\eta}{k_B T}\right\}^{2/3} \frac{D_t}{D_r^{1/3}} = \frac{\ln(P_{DDLS}) + C_t}{(\ln(P_{DDLS}) + C_r)^{1/3}} \quad (3)$$

where,

$$C_t = 0.312 + 0.565P_{DDLS}^{-1} - 0.100P_{DDLS}^{-2} \quad (4)$$

$$C_r = -0.662 + 0.917P_{DDLS}^{-1} - 0.050P_{DDLS}^{-2} \quad (5)$$

The numerical value obtained for $f(P_{DDLS})$ by substituting a value for P_{DDLS} into the right-hand side of eq 3 must be equal to the numerical value of $f(P_{DDLS})$ obtained by substituting D_t and D_r, both obtained experimentally.

D_t and D_r were obtained from the correlation functions using the global fits for the three gold rod samples and are given in Table 2. The relation between D_t and D_r and P_{DDLS}, given by eq 3, is represented graphically in Figure 3. The calculated hydrodynamic aspect ratio for Au-nanorod-1 as obtained using DDLS agrees with the earlier provided estimate for P_{TEM}. The expected increase of hydrodynamic aspect ratio for Au-nanorod-2 and -3 is not recovered by the DDLS analysis. For these particles, the measurements in Figure 1C showed that the corresponding LSPR modes lead to only a small extinction coefficient at the wavelength used in the light-scattering experiments (647 nm). The weaker scattering arising from the LSPRs shifts leads to a worsened signal-to-noise ratio. Additionally, DDLS analysis does not take polydispersity into account, which may induce a systematic error weighing more the particles that scatter or absorb strongly. On the basis of the sensitivity in measurement errors and the possible errors induced by the effects of polydispersity, the hydrodynamic aspect ratio obtained from DDLS can show large deviations as compared to the values (P_{TEM}) estimated from TEM.

In this respect it should be noted that P_{DDLS} is inside the logarithm in eq 3. A simplified sensitivity analysis can be used to estimate the effect of small variations in D_t and D_r on the calculated hydrodynamic aspect ratio. A detailed 3D plot of P_{DDLS} as a function of D_t and D_r, in Figure 3, shows that an error in D_t has a larger effect on the aspect ratio of the particles as compared to an error in D_r. This is assuming that the errors in D_t do not affect the errors in D_r. For the aspect ratios considered here, a 5% error in both D_t and D_r, a typical value for dynamic light-scattering measurements, which includes experimental errors and errors in curve fitting, translates into a 30−40% error in the calculated aspect ratio, as shown by the error lines in Figure 3. It should be pointed out that for large aspect ratio particles the error in the aspect ratio determined by DDLS would be smaller. Finally, the samples are somewhat polydisperse, and it is hard to assess the effect of shape and size polydispersity; while purely elastic scattering will be dominated by the larger particles, the surface plasmon modes dictate a more complex dependence on particle size and shape.[24]

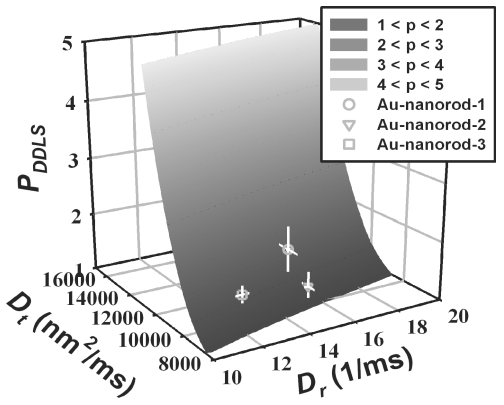

Figure 3. 3D plot of aspect ratio (P_{DDLS}) as a function of translational diffusion (D_t) and rotational diffusion (D_r) coefficients following eq 3. The symbols are experimentally determined values of D_t and D_r and the corresponding P_{DDLS}. The bars represent the measurement errors on D_t, and D_r and the subsequent error on the calculated P_{DDLS}.

The analysis of the DDLS data for Au-decas is even more complex due to the different polarization directions of the scattered light by the decahedron-shaped particles, especially in the presence of the corresponding surface plasmon modes. The expressions for normalized intensity autocorrelation functions for disks of complex shapes are not currently available. This disadvantage of DDLS, as with any method that employs scattering, is that the relationship between the scattering intensity and the correlation function needs to be known *a priori* for particles with different shapes and polydispersity, which are not known beforehand.

Rheo-optical Measurements. To circumvent some of the inherent limitations of DDLS, the use of rheo-optical measurements has been explored. First, in rheo-optics a well-defined flow field is used, which determines the particle motion and leads to a simpler relation between aspect ratio and the observed optical response, as will be discussed below. Second, the measured dichroism is determined by both the scattering and absorption of the particles, hence leading to a more pronounced optical response for the gold nanoparticles. The quantitative calculation of dichroism for these small gold particles is even more difficult compared to the scattering properties, and using dichroism to back-calculate for example polydispersity effects is not trivial. However, regardless of the detailed optical response, the principal axis of the optical anisotropy is determined by the shape of the particle. The evolution of the average orientational angle of the particles can hence be monitored. The orientation angle is not dependent on scattering theory and the associated complicated effects of polydispersity unlike the scattering or absorption properties, and hence its magnitude does not directly depend on the size of the particles. Following earlier work for scattering dichroism,[37,38] the time evolution of the orientation distribution function can be used to determine the aspect ratio of the particles.

For monodisperse rods, the orientation distribution function upon inception of flow at high Péclet numbers will be an oscillatory function in time. The tumbling motion of the individual particles follows Jeffery orbits,[39] with velocities that vary with orientation, slowing down when they come close to being oriented in the flow direction. As a consequence, the optical properties corresponding to the orientation distribution, such as linear dichroism, will oscillate in time. When polydispersity of the hydrodynamic aspect ratio, stemming from both size and shape, is present, the oscillatory behavior of the ODF upon start-up of flow will be damped due to phase mixing.[37] The decay of orientation angle to a constant value due to phase mixing is a quantitative measure of the degree of polydispersity, higher values resulting in a faster decay.

Starting with the motion of a single particle, the time evolution of the ODF and the average orientation angle can be developed. The creeping flow equation for spheroidal particles in a Newtonian fluid subject to simple shear flow was solved by Jeffery.[39] The forces acting on a spheroid can be reduced to two torques, due to which particles tumble in flow. In a simple shear flow the evolution equation of the orientation of the major axis of an individual, non-Brownian, neutrally buoyant spheroid with aspect ratio P_D describes a motion given by

$$\tan\theta = \frac{CP_D}{(P_D{}^2\cos^2\phi + \sin^2\phi)^{0.5}} \quad (6)$$

$$\tan\phi = P_D \tan\left\{\frac{2\pi t}{T} + \kappa\right\} \quad (7)$$

where θ and ϕ are the first and second Euler angles. C and κ are constants of integration determined by the initial conditions. T is the period of rotation determined by the particle aspect ratio (P_D, as measured using dichroism) and shear rate ($\dot{\gamma}$).

$$T = \frac{2\pi}{\dot{\gamma}}\left\{P_D + \frac{1}{P_D}\right\} \quad (8)$$

For the motion of any rigid axis-symmetric body, Breherton[40] obtained a similar equation to Jeffery's (eq 8) where P_D was the equivalent hydrodynamic aspect ratio. It has to be noted that the aspect ratios for Au-decas are calculated assuming that they are oblate ellipsoids. Since Au-decas have well-defined faces, the true volume of an Au-deca will be smaller than that calculated by treating it as an equivalent oblate ellipsoid, and consequently a smaller value of the aspect ratio is expected from the rheo-optical measurements.

The hydrodynamic aspect ratio has been determined from experimental measurements of either turbidity,[41] scattering dichroism,[37,42,43] or UV−vis absorption.[17] In the present case of the gold particles the dichroism arises from both scattering and intrinsic dichroism contributions, but these are assumed to be coaxial. Dichroism and orientation angle are simultaneously calculated from the harmonic coefficients (see Materials and Methods section). The extinction coefficient δ'' is given in the monograph by Fuller as[16]

$$\delta'' = -\mathrm{sgn}(R_2)\tanh^{-1}\left\{\frac{1}{2}\sqrt{\frac{R_1}{-J_1(A)} + \frac{R_2}{-J_2(A)}}\right\} \quad (9)$$

where J_1(A) and J_2(A) are Bessel functions of the zeroth order. The dichroism is related to the extinction coefficient by

$$\Delta n'' = \frac{\delta''\lambda}{2\pi l} \quad (10)$$

where l is the optical path length and λ is the wavelength of the light source. The magnitude of dichroism is related to the average orientation of the particles induced by flow. In the steady state, the average dichroism and orientation angle of all the particles are constant, and on average the particles spend more time along the flow direction. To obtain polydispersity it is necessary to measure the phase mixing in the ODF that occurs under transient flow conditions.

To obtain the hydrodynamic aspect ratio and the associated polydisperisty, a nonlinear fit to the time-dependent average ODF is used as developed by Vermant *et al.*[38] For particles with small aspect ratio an expression for the orientation angle as a function of aspect ratio and polydispersity is given by

$$\tan 2\chi = \frac{2\int_0^\infty (P_D - P_D{}^{-1})\sin\frac{4\pi t}{T} g(P_D)\,dP_D}{\int_0^\infty \left\{P_D{}^2 - P_D{}^{-2} - (P_D{}^2 - P_D{}^{-2})\cos\frac{4\pi t}{T}\right\} g(P_D)\,dP_D} \quad (11)$$

where $g(P_D)$ is assumed to be a Gaussian distribution function of the hydrodynamic aspect ratio

$$g(P_D) = \frac{1}{\sqrt{2\pi\sigma^2}}\exp\left\{\frac{-(P_D - \bar{P}_D)^2}{2\sigma_D{}^2}\right\} \quad (12)$$

and T is the period of rotation, given by eq 8. Using eq 11, the average hydrodynamic aspect ratio ($\bar{P}_D$) and the corresponding polydispersity (σ_D) can be determined. The approximate analytical formula is valid only for small anisotropies and a Gaussian distribution of aspect ratios. If needed, the full set of equations can be solved numerically and inverted (see for example ref 38).

The set of equations describing the evolution of the ODF in transient flow are only valid in the flow regime where rotational Brownian motion is dominated by the convective forces, *i.e.*, the high Péclet number regime. To determine this regime, the steady-state properties need to be measured first. As an example of typical

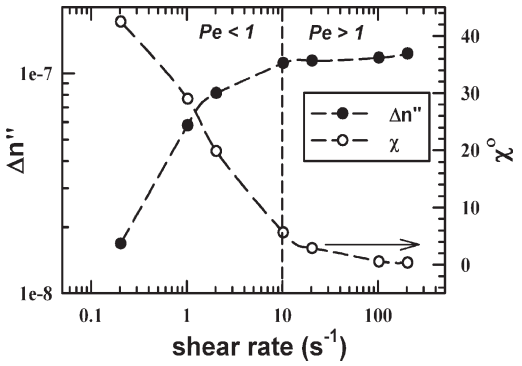

Figure 4. Dichroism and orientation angle as a function of shear rate for Au-deca-2 in 99.5% glycerol.

experimental results of the evolution of the steady-state dichroism and the average orientation angle, results are given for a suspension of Au-deca-2 in Figure 4. At low shear rates, due to the dominance of rotational Brownian motion, the distribution of orientations remains close to isotropic, the magnitude of dichroism is small, and the average orientation angle is still large. When the shear rate is increased, the hydrodynamic forces become dominant and tumbling particles spend most of their orbit in an orientation close to the flow direction. On average, the orientation of the particles' long axis is close to the flow direction and the magnitude of dichroism increases as shown in Figure 4. The critical shear rate at which the hydrodynamic forces become dominant is taken as the lower limit for the transient experiments.

In the transient experiments, flow is started above the critical shear rate for a suspension that has been rendered isotropic by the effects of Brownian motion. When flow is started in the high Péclet regime, the tumbling of the particles causes the transient response to show an oscillatory response of the dichroism (data not shown) and orientational angle, shown in Figure 5 (Au-nanorods) and Figure 6 (Au-decas). The oscillatory response is damped because particles with different aspect ratios have different tumbling periods, and hence phase mixing occurs. The phase mixing is least pronounced for Au-deca-3, as expected on the basis of the polydispersity estimates from the TEM images. For the other two sizes of decahedral particles the damping is of the same extent. The signal-to-noise ratio for the Au-decas is good, due to the high extinction value of light at 632.8 nm due to the LSPR (Figure 1D). Similar results are obtained for Au-nanorods, Figure 1C, but the S/N ratio is worse. For Au-nanorod-2, due to the low extinction value, the measured transient signal contains a large amount of noise associated with the signal (Figure 5B). Finally, for the long aspect ratio Au-nanorod-3, the light extinction value at 632.8 nm is extremely low and the diameter is small, due to which we could not measure any reliable signal. Table 3 shows a list of hydrodynamic aspect ratios measured from

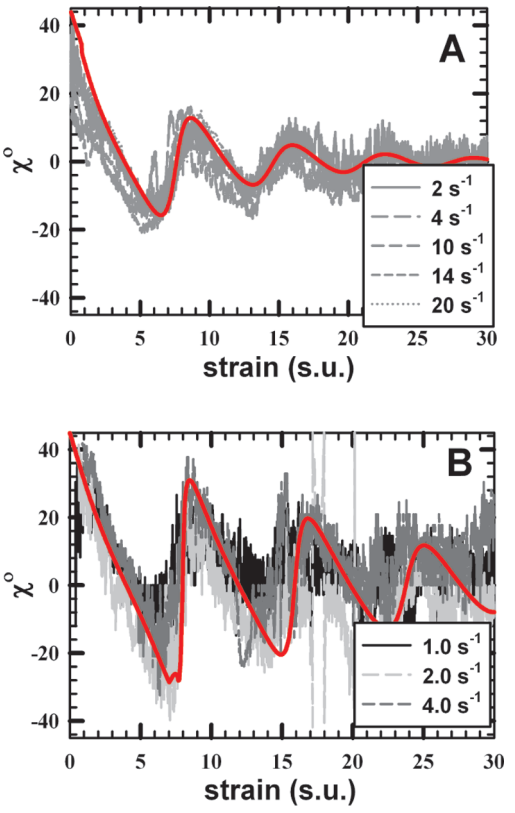

Figure 5. Orientation angle as a function of strain for (A) Au-nanorod-1 and (B) Au-nanorod-2.

dichroism and the corresponding polydispersity obtained by nonlinear fits of eq 11 to the transient data.

Table 4 compares the aspect ratios of gold nanoparticles obtained from different methods. TEM data are typically taken as the standard method, but as the sample preparation is rather labor intensive, it is often not possible to acquire the number of images required to obtain statistically relevant data. Moreover, the fact that a surfactant or polymer layer thickness needs to be estimated to obtain the hydrodynamic aspect ratio adds to the uncertainty of P_{TEM}, even beyond the statistical uncertainty in column 3 of Table 4. Optical methods used to determine the hydrodynamic properties such as DDLS and dichroism require simpler sample preparation, and the equipment is also simple. However, DDLS turns out to be prone to errors, mainly due to the functional form of the dependence of P_{DDLS} on D_t. Many authors have used DDLS to measure hydrodynamic aspect ratios and have found large differences between microscopy techniques and DDLS. For instance, Rodríguez-Fernández *et al.*[33] measured hydrodynamic aspect ratios of gold rods that qualitatively agree with the calculated P_{TEM}. If, however, the hydrodynamic aspect ratio is computed from eq 3 using their data, we see that values of P_{DDLS} are almost 50% smaller than those estimated from P_{TEM}, even when the CTAB layer thickness is added.[33] Similarly, hydrodynamic aspect ratios for single-walled carbon

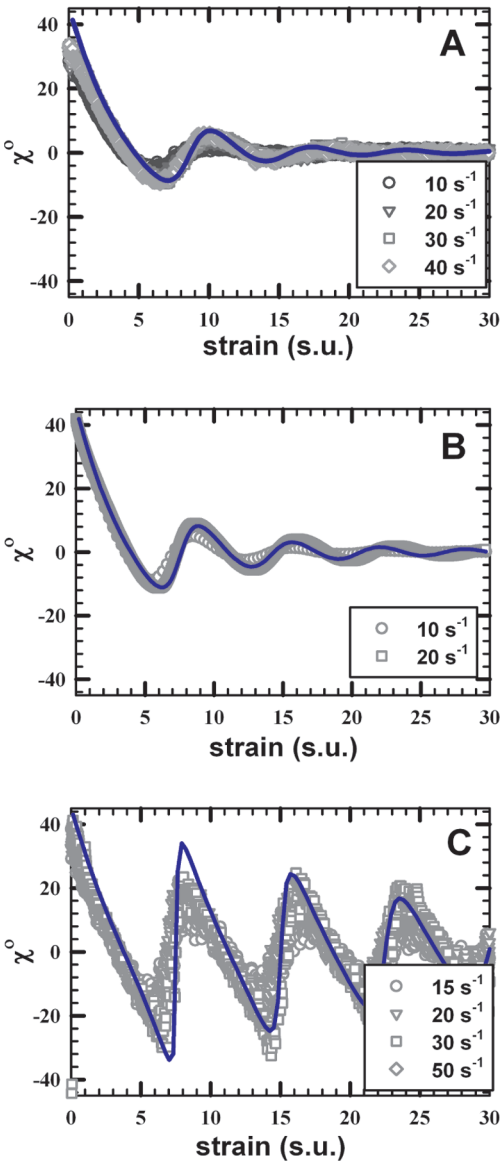

Figure 6. Orientation angle as a function of strain for (A) Au-deca-1, (B) Au-deca-2, and (C) Au-deca-3.

TABLE 3. Hydrodynamic Aspect Ratio and the Corresponding Polydispersity of Gold Nanoparticles Obtained from Flow Startup Dichroism Experiments

sample	P_D	σ_D
Au-nanorod-1	1.7 ± 0.1	0.14 ± 0.03
Au-nanorod-2	2.0 ± 0.1	0.05 ± 0.02
Au-deca-1	0.47 ± 0.03	0.17 ± 0.04
Au-deca-2	0.55 ± 0.02	0.16 ± 0.03
Au-deca-3	0.55 ± 0.01	0.05 ± 0.01

nanotubes calculated from DDLS measurements gave almost an order of magnitude differences when compared with AFM results.[44] The large uncertainty on P_{DDLS} renders further analysis of polydispersity meaningless. DDLS is only useful for rod-like particles, as detailed scattering theories are required to analyze the data. In contrast, the rheo-optical method relies only on the time evolution of the optical axis of the axisymmetric particles,[38,40] and due to the use of a well-defined flow field, the tumbling period is linked in a simple manner to P_D. The robust link between P_D and the tumbling period, which may be valid for all methods that employ external fields to control particle motions instead of relying on Brownian motion, makes the analysis in terms of polydispersity possible. It should be noted that for particles with a large aspect ratio the tumbling period becomes difficult to measure and the drawbacks of DDLS become less severe. Finally it should be noted that the flow dichroism method still requires sufficient optical response, which for nanoparticles limits this technique to samples with adequately strong optical response such as gold particles. Finally, although we did not pursue this here, once the aspect ratio is known, the size of the particles can be estimated from the relaxation of the dichroism upon cessation of flow. This then provides a value for the rotational diffusivity that can be used to calculate an effective size, similar to the DDLS results. For example, rotational diffusivities of 0.23 s^{-1} were obtained for Au-deca-2 from the relaxation of the dichroism in 99.5% glycerol. From the above rotational diffusivity an equivalent size of L = 197 nm and d = 108 nm was obtained using the Perrin equation for an equivalent ellipsoid.[45]

TABLE 4. Aspect Ratio of Gold Nanoparticles Estimated from TEM and Measured Using DDLS and Flow Dichroism along with the Polydispersity Obtained from Flow Dichroism

sample	AR[a]	P_{TEM}	P_{DDLS}	P_D	σ_D
Au-nanorod-1	2.80 ± 0.8	2.3 ± 0.55	1.85 ± 0.65	1.7 ± 0.1	0.14 ± 0.03
Au-nanorod-2	3.40 ± 0.5	2.7 ± 0.35	1.35 ± 0.47	2.0 ± 0.1	0.05 ± 0.02
Au-nanorod-3	4.40 ± 1.1	3.4 ± 0.56	1.55 ± 0.54	NA	NA
Au-deca-1	0.62 ± 0.06	0.63 ± 0.04	NA	0.47 ± 0.03	0.17 ± 0.04
Au-deca-2	0.62 ± 0.07	0.63 ± 0.06	NA	0.55 ± 0.02	0.16 ± 0.03
Au-deca-3	0.62 ± 0.02	0.62 ± 0.02	NA	0.55 ± 0.01	0.05 ± 0.01

[a] Geometric aspect ratio.

CONCLUSIONS

The aspect ratios of gold nanoparticles with various morphologies were measured by three different methods, and the results critically compared. Transmission electron microscopy provides a geometric aspect ratio, but good statistics can be obtained only with substantial effort. Optical methods on particles in suspension, such as DDLS and rheo-optics, provide hydrodynamic aspect ratios. From DDLS, correlation functions are simple to measure, but the analysis to determine hydrodynamic aspect ratios is rather complex. Moreover, a small error in measuring diffusion coefficients results in a large error in the calculated hydrodynamic aspect ratio. Rheo-optics provides a

more robust result for small aspect ratio particles along with the associated polydispersity. The better results obtained from the rheo-optical method arise from the use of a well-defined flow field, which unlike Brownian motion can be applied in a precise and controlled way and due to using the evolution of the orientation angle. The latter is less affected by the effects of size and shape polydispersity compared to absolute quantities such as scattering intensity and absorption. The orientation angle properly reflects the average of the distribution. We also showed that by using dichroism even on complex shaped nanoparticles the effective hydrodynamic aspect ratio can be readily determined. The only drawback of rheo-optics is that the particles must be suspended in a high-viscosity fluid and they should provide a sufficient optical signal for linear dichroism to be detected, either by scattering or by absorption.

MATERIALS AND METHODS

Synthesis of Gold Particles. Tetrachloroauric acid ($HAuCl_4 \cdot 3H_2O$), sodium borohydride ($NaBH_4$), sodium chloride (NaCl), HCl, cetyltrimethylammonium bromide (CTAB), and ascorbic acid were purchased from Aldrich. Poly(vinylpyrrolidone) (PVP, MW 10 000, 40 000) and *N*,*N*-dimethylformamide (DMF) were supplied by Fluka. All chemicals were used as received. Pure grade ethanol and Milli-Q grade water were used to make up all solutions.

Gold nanorods were prepared following the Ag^+-assisted method proposed by Nikoobakht *et al.*[46] and modified by Liu *et al.*[47] Briefly, first a gold seed solution was prepared by borohydride reduction of 5 mL of 0.25 mM $HAuCl_4$ in an aqueous 0.1 M CTAB solution. For the synthesis of gold nanorods, 24 μL of seed solution was added to 10 mL of a growth solution containing 0.1 M CTAB, 0.5 mM $HAuCL_4$, 0.75 mM ascorbic acid, and 0.12 mM silver nitrate and in the presence of 0.019 M HCl and 0.01 M HCl and in the absence of HCl, which resulted in gold rods with geometric aspect ratios of 2.8, 3.4, and 4.4, respectively.

A detailed procedure of the synthesis of gold decahedrons is given in refs 48 and 49. For the synthesis of decahedral Au nanoparticles (Au-deca-1), the seed gold nanoparticles with 2−3 nm size were prepared following a procedure previously reported in ref 45. Briefly, 22 μL of an aqueous solution of 0.1136 M HAuCl4 was added to 47.5 mL of a solution in a H_2O−DMF mixture (1:18 v/v) containing 0.017 g of PVP (MW 10 000). Then, 2.5 mL of a freshly prepared 10 mM $NaBH_4$ solution was injected quickly into the solution under vigorous stirring. The gold sol was stirred for 2 h at room temperature. The seed was not used until 24 h after preparation to allow for complete $NaBH_4$ decomposition and to avoid further nucleation. Prior to seed addition, 0.825 mL of 0.1136 M $HAuCl_4$ aqueous solution was added to 15 mL of a PVP (MW 40 000) 2.5 mM solution in DMF in a 50 mL vessel, and the mixture was ultrasonically irradiated until complete disappearance of the Au^{3+} CTTS absorption band at 325 nm. Then, 1 mL of the preformed seed solution ([Au] = 5×10^{-5} M) was added and sonicated further for complete reduction, indicated by no further red-shift of the plasmon band.

The decahedral nanoparticles Au-deca-2 and Au-deca-3 were obtained using Au-deca-1 decahedral nanoparticles as seeds. The procedure is similar to that presented for small decahedra; that is, prior to seed addition, a certain amount (0.452 and 1.4 mL to obtain Au-deca-2 and Au-deca-3 particles, respectively) of 0.1037 M $HAuCl_4$ aqueous solution was added to 15 mL of a 2.5 mM PVP (MW 40 000) solution in DMF, and the mixture was ultrasonically irradiated in a 50 mL vessel until complete disappearance of the Au^{3+} CTTS absorption band at 325 nm. Then, 0.8 mL of seed solution ([Au] = 6.3×10^{-4} M) was added and sonicated further for complete reduction.

TEM micrographs and the corresponding light extinction spectra for gold nanorods and gold decahedrons are shown in Figure 1.

DDLS. Time autocorrelation functions of the scattered intensity $g_2(q,t)$ were recorded with a standard DLS apparatus equipped with a Krypton ion (Kr^+) laser (λ_o = 647 nm, 100 mW). The scattering angle, θ, was varied from 40° to 130° in steps of 5° covering a range of 8.835×10^{-3} nm < q < 2.34×10^{-2} nm, where $q = (4\pi n_s/\lambda) \sin(\theta/2)$ is the scattering vector. The polarization state of incident and scattered light was controlled with a $\lambda/2$ plate and a polarizer in the primary beam and an analyzer in the scattered beam (all polarizing optics are from Bernhard Halle Nachfl, Berlin, Germany). The scattered light was collected with a monomode optical fiber (OZ-Optics,Ottawa, Canada) and detected with a SO-SIPD dual photomultiplier unit by ALV Laserverstriebsgesellschaft mbH, Langen, Germany. The transistor−transistor logic output of the avalanche diode was processed in the cross-correlation mode of a multiple tau correlator, ALV-5000. The shortest delay time, which is reliably accessible with this detector−correlator combination, is ~100 ns. For each sample, a complete angular set of correlation functions was recorded in both vertical−vertical and vertical−horizontal modes. DDLS experiments were performed on suspensions containing gold particles in water instead of glycerol (which is used in dichroism experiments) because the time needed to obtain a good autocorrelation function for a glycerol system was close to 24 h per angle as compared to 2 h for a water system. One set of experiments for gold rods in glycerol was measured and compared to the same gold particles in water. When corrected for the medium viscosity, the values between gold rods in water and glycerol were identical.

Dichroism. Dichroism measurements have been performed using a MCR300 controlled-stress rheometer (Paar Physica, Austria) as a mechanical platform and using an in-house-developed optical train.[50] To monitor tumbling of anisotropic particles in the vorticity plane, a Couette cell was used. The inner and outer radii of the Couette cell are 16.95 and 17.95 mm (R_i/R_o = 0.94), respectively, and the height of the cylinder was 21 mm. Experiments were performed at room temperature. To reduce the effect of Brownian motion and to be in a high Péclet regime, gold nanoparticles were suspended in 99.5% glycerol (Sigma). The optical train consisted of a He−Ne laser source (λ = 632.8 nm, 10 mW), followed by a Glan-Thompson polarizer (P1, Newport, USA), a photoelastic modulator (PEM, Beaglehole Instruments, New Zealand) oriented at 45° with respect to P1, and a zero-order quarter-wave plate (Newport) at 0° with respect to P1. The beam is then passed into the Couette cell in the vorticity plane, and the scattered light is collected by a photodiode. Data from the photodiode is sent through a low-pass filter, and the harmonic contents are passed to two lock-in amplifiers (Stanford Research Systems model 530), which gives the first and the second harmonic (R_1 and R_2) as the output. The setup was calibrated in such a manner that the orientation in the flow direction corresponded to a positive dichroism. The concentration was chosen to be large enough to ensure a sufficient signal-to-noise ratio for the harmonic components R_1 and R_2, yet small enough to be in the single-scattering limit and to remain in the hydrodynamically dilute regime. R_1 and R_2 along with calibration values for $J_1(A)$ and $J_2(A)$ are used to obtain the magnitude of the dichroism and the associated orientation angle.

Acknowledgment. The authors thank Dr. P. Holmqvist for useful discussions. We thank the EU for funding through the project NANODIRECT (Grant No. CP-FP 213948-2).

REFERENCES AND NOTES

1. Glotzer, S. C.; Solomon, M. J. Anisotropy of Building Blocks and their Assembly into Complex Structures. *Nat. Mater.* **2007**, *6*, 557–562.
2. Shipway, A. N.; Katz, E.; Willner, I. Nanoparticles Arrays on Surfaces for Electronic, Optical, and Sensor Applications. *ChemPhysChem* **2000**, *1*, 18–52.
3. Gangopadhyay, R.; De, A. Conducting Polymer Nanocomposites: A Brief Overview. *Chem. Mater.* **2000**, *12*, 608–622.
4. Hao, E.; Schatz, G. C.; Hupp, J. T. Synthesis and Optical Properties of Anisotropic Metal Nanoparticles. *J. Fluoresc.* **2004**, *14*, 331–340.
5. Pérez-Juste, J.; Pastoriza-Santos, I.; Liz-Marzán, L. M.; Mulvaney, P. Gold Nanorods: Synthesis, Characterization and Applications. *Coord. Chem. Rev.* **2005**, *249*, 1870–1901.
6. Law, M; Sirbuly, D. J.; Johnson, J. C.; Goldberger, J.; Saykally, R. J.; Yang, P. Nanoribbon Waveguides for Subwavelength Photonics Integration. *Science* **2004**, *305*, 1269–1273.
7. Hadjipanayis, G. C. Nanophase Hard Magnets. *J. Magn. Magn. Mater.* **1999**, *200*, 373–391.
8. Elson, E. L. Cellular Mechanics as an Indicator of Cytoskeletal Structure and Function. *Annu. Rev. Biophys. Biophys. Chem.* **1988**, *17*, 397–430.
9. Lin, Y. C.; Koenderink, G. H.; MacKintosh, F. C.; Weitz, D. A. Viscoelastic Properties of Microtubule Networks. *Macromolecules* **2007**, *40*, 7714–7720.
10. Jana, N. R. Shape Effect in Nanoparticle Self-Assembly. *Angew. Chem., Int. Ed.* **2004**, *43*, 1536–1540.
11. Grzelczak, M.; Vermant, J.; Furst, E. M.; Liz-Marzán, L. M. Directed Self-Assembly of Nanoparticles. *ACS Nano* **2010**, *4*, 3591–3605.
12. Onsager, L. The Effects of Shape on the Interaction of Colloidal Particles. *Ann. N.Y. Acad. Sci.* **1949**, *51*, 627–659.
13. Goldstein, J.; Newbury, D. E.; Joy, D. C.; Lyman, C. E.; Echlin, P.; Lifshin, E.; Sawyer, L.; Michael, J. R. *Scanning Electron Microscopy and X-ray Microanalysis*; Springer: New York, 2003.
14. Russel, W. B.; Saville, D. A.; Schowalter, W. R. *Colloidal Dispersions*; Cambridge University Press: Cambridge, 1989.
15. Pérez-Juste, J.; Rodriguez-Gonzalez, B.; Mulvaney, P.; Liz-Marzán, L. M. Optical Control and Patterning of Gold-Nanorod-Poly(vinyl alcohol) Nanocomposite Films. *Adv. Funct. Mater.* **2005**, *15*, 1065–1071.
16. Fuller, G. G. *Optical Rheometry of Complex Fluids*; Oxford University Press: Oxford, 1995.
17. Sader, J. E.; Pepperell, C. J.; Dunstan, D. E. Measurement of the Optical Properties and Shape of Nanoparticles in Solution using Couette Flow. *ACS Nano* **2008**, *2*, 334–340.
18. Wilcox, C. D.; Dove, S. B.; McDavid, W. D.; Greer, D. B. *UTHSCSA Image Tool*; Department of Dental Diagnostic Science at The University of Texas Health Science Center: San Antonio, TX, 1996.
19. Weisstein, E. W. Pentagonal Dipyramid. *From Math World—A Wolfram Web Resource.*
20. Tanford, C. *The Hydrodynamic Effect*; Wiley: New York, 1973.
21. Kekicheff, P.; Richetti, P. Direct Measurement of Interactions in Supermolecular Fluids and Liquid Crystals. *Pure Appl. Chem.* **1992**, *64*, 1603–1609.
22. Smith, J. N.; Meadows, J.; Williams, P. A. Adsorption of Polyvinylpyrrolidone onto Polystyrene Latices and the Effect on Colloid Stability. *Langmuir* **1996**, *12*, 3773–3778.
23. Gonzalez, A. L.; Reyes-Esqueda, J. A.; Noguez, C. Optical Properties of Elongated Noble Metal Nanoparticles. *J. Phys. Chem. C* **2008**, *112*, 7356–7362.
24. Ni, W. H.; Zhou, X.; Wang, J. Tailoring Longitudinal Surface Plasmon Wavelengths, Scattering and Absorption of Gold Nanorods. *ACS Nano* **2008**, *2*, 677–686.
25. Berne, B. J.; Pecora, R. *Dynamic Light Scattering: With Applications to Chemistry, Biology, and Physics*; Dover Publications, 2000.
26. Einstein, A. On the Movement of Small Particles Suspended in Stationary Liquid Required by the Molecular-Kinetic Theory of Heat. *Ann. Phys.* **1905**, *17*, 549–560.
27. Sutherland, W. A. Dynamical Theory of Diffusion for Non-Electrolytes and the Molecular Mass of Albumin. *Philos. Mag. S. 6* **1905**, *9*, 781–785.
28. Droegemeier, J.; Eimer, W. Polarized and Depolarized Dynamic Light Scattering Study on F-Actin in Solution: Comparison with Model Calculations. *Macromolecules* **1994**, *27*, 96–101.
29. Lehner, D.; Lindner, H; Glatter, O. Determination of the Translational and Rotational Diffusion Coefficients of Rod-like Particles Using Depolarized Dynamic Light Scattering. *Langmuir* **2000**, *16*, 1689–1695.
30. Piazza, R.; Degiorgio, V. Dynamic Light Scattering Study of Colloidal Crystals Made of Anisotropic Spherical Latex Particles. *Phys. A* **1992**, *182*, 576–592.
31. Shah, D.; Fytas, G.; Vlassopoulos, D.; Di, J.; Sogah, D.; Giannelis, E. P. Structure and Dynamics of Polymer-Grafted Clay Suspensions. *Langmuir* **2005**, *21*, 19–25.
32. Haro-Perez, C.; Andablo-Reyes, E.; Diaz-Leyva, P.; Arauz-Lara, J. L. Microrheology of viscoelastic fluids containing light-scattering inclusions. *Phys. Rev. E* **2007**, *75*, 0415051–6.
33. Rodríguez-Fernández, J.; Pérez-Juste., J.; Liz-Marzán, L. M.; Lang, P. R. Dynamic Light Scattering of Short Au Rods with Low Aspect Ratios. *J. Phys. Chem. C* **2007**, *111*, 5020–5025.
34. Boersma, J. Viscous Force Constant for a Closed Cylinder. *J. Chem. Phys.* **1964**, *32*, 1626–1632.
35. Brenner, H. Rheology of a Dilute Suspension of Axisymmetric Brownian Particles. *Int. J. Multiphase Flow* **1974**, *1*, 195–341.
36. Ortega, A.; Garcia de la Torre, J. Hydrodynamic Properties of Rodlike and Disklike Particles in Dilute Solution. *J. Chem. Phys.* **2003**, *119*, 9914–9919.
37. Frattini, P. L.; Fuller, G. G. The Dynamics of Dilute Colloidal Suspensions Subject To Time-Dependent Flow-Fields by Conservative Dichroism. *J. Colloid Interface Sci.* **1984**, *2*, 506–518.
38. Vermant, J.; Yang, H.; Fuller, G. G. Rheo-optical Determination of Aspect Ratio and Polydispersity of Nonspherical Particles. *AIChE J.* **2001**, *47*, 790–798.
39. Jeffery, G. B. The Motion of Ellipsoidal Particles Immersed in a Viscous Fluid. *Proc. R. Soc. London, Ser. A* **1922**, *102*, 161–179.
40. Breherton, F. P. The Motion of Rigid Particles in a Shear Flow at Low Reynolds Number. *J. Fluid Mech.* **1962**, *14*, 284–304.
41. Meeten, G. H. Conservative Dichroism in the Rayleigh-Gans-Debye Approximation. *J. Colloid Interface Sci.* **1981**, *84*, 235–239.
42. Frattini, P. L.; Fuller, G. G. Conservative Dichroism of a Sheared Suspension in the Rayleigh-Gans Light-Scattering Approximation. *J. Colloid Interface Sci.* **1987**, *119*, 335–351.
43. Johnson, S. J.; Fuller, G. G. The Optical Anisotropy of Sheared Hematite Suspensions. *J. Colloid Interface Sci.* **1988**, *124*, 441–451.
44. Shetty, M. A.; Wilkins, G. M. H.; Nanda, J.; Solomon, M. J. Multiangle Depolarized Dynamic Light Scattering of Short Functionalized Single-Walled Carbon Nanotubes. *J. Phys. Chem. C* **2009**, *113*, 7129–7133.
45. Strackee, L. Rotational Diffusion of Rhodopsin-Digitonin Micelles Studied by Transient Photodichroism. *Biophys. J.* **1971**, *11*, 728–738.
46. Nikoobakht, B.; El-Sayed, M. A. Preparation and Growth Mechanism of Gold Nanorods (NRs) Using Seed-Mediated Growth Method. *Chem. Mater.* **2003**, *15*, 1957–1962.
47. Liu, M.; Guyot-Sionnest, P. Mechanism of Silver(I)-Assisted Growth of Gold Nanorods and Bipyramids. *J. Phys. Chem. B* **2005**, *109*, 22192–22200.
48. Pastoriza-Santos, I.; Sanchez-Iglesias, A.; Garcia de Abajo, F. J.; Liz-Marzán, L. M. Environmental Optical Sensitivity of Gold Nanodecahedra. *Adv. Funct. Mater.* **2007**, *17*, 1443–1450.
49. Teranishi, T.; Kiyokawa, I.; Miyake, M. Synthesis of Monodisperse Gold Nanoparticles Using Linear Polymers as Protective Agents. *Adv. Funct. Mater.* **1998**, *8*, 596–599.
50. Pellens, L.; Vermant, J.; Mewis, J. Deviations from the Stress-Optical Relation in Telechelic Associative Polymer Solutions. *Macromolecules* **2005**, *38*, 1911–1918.